ELSEVIER

International Journal of Heat and Fluid Flow 21 (2000) 312–319

International Journal of
HEAT AND
FLUID FLOW

www.elsevier.com/locate/ijhff

Accuracy and robustness of nonlinear eddy viscosity models

W. Bauer [1], O. Haag *, D.K. Hennecke

Gas Turbines and Flight Propulsion, Darmstadt University of Technology, Petersenstrasse 30, D-64287 Darmstadt, Germany

Received 6 September 1999; accepted 6 January 2000

Abstract

Two nonlinear eddy viscosity models (EVMs) proposed by Shih et al. (Shih, T.H., Zhu, J., Lumley, J.L., 1995. Comput. Methods Appl. Mech. Engrg. 125, 287–302) and Craft et al. (Craft, T.J., Launder, B.E., Suga, K., 1996. Int. J. Heat Fluid Flow 17, 108–115) and one algebraic Reynolds stress model of Gatski and Speziale (Gatski, T.B., Speziale, C.G., 1993. J. Fluid Mech. 254, 59–78) are compared to the standard k–ϵ model and the Reynolds stress model of Launder et al. (Launder, B.E., Reece, G.J., Rodi, W., 1975. J. Fluid Mech. 68, 537–566) with respect to model accuracy and computational robustness. Three flow situations are considered to analyze the models' capabilities in flows with streamline curvature: A backward facing step flow (Driver, D.M., Seegmiller, H.L., 1985. AIAA J. 23, 163–171), a plane U-duct flow (Monson, D.J., Seegmiller, H.L., 1992. NASA Technical Memorandum, 103931) and a curved mixing layer (Castro, I.P., Bradshaw, P., 1976. J. Fluid Mech. 73, 265–304). Results indicate that an improved prediction of the flow fields especially for important flow features like recirculation zones can be obtained with the tested models compared to calculations with the standard k–ϵ model. The decrease of computational robustness compared to the calculations with the standard k–ϵ model is rather moderate once a quasi-linear form of the models is employed.

Keywords: Turbulence modeling; Streamline curvature

1. Introduction

The majority of turbulent flow calculations is carried out using linear eddy viscosity models (EVMs) like the well-known k–ϵ model, although those models fail in predicting turbulent flows with streamline curvature or with respect to rotating frame of reference and for the prediction of secondary flows in non-circular channels. The reason for the popularity of linear EVMs despite their weaknesses in more complex flow situations is their computational efficiency and robustness. This is especially important when using CFD as a design tool for technical applications. Second moment closures can overcome the limitations of the linear EVMs is in more complex flows because they account for curvature and rotation effects on turbulence. But since these schemes require six additional transport equations for the Reynolds stresses to be solved they cannot compete with EVMs with respect to computational robustness and efficiency. Therefore nonlinear EVMs and algebraic Reynolds stress models were developed to combine computational robustness and efficiency of linear EVMs with improved model accuracy of second moment closures. The first model considered here is the nonlinear EVM proposed by Shih et al. (1995). In this model the general polynomial ansatz of a Reynolds stress–strain relationship is truncated at second power terms. The coefficients are calibrated by rapid distortion theory and realizability arguments. The second nonlinear EVM considered is from Craft et al. (1996) (CLS). Additional cubic terms are used in the CLS model to account properly for the effects of streamline curvature. Gatski and Speziale (1993) (GS) used a different approach for the development of their turbulence model. They derived an explicit algebraic Reynolds stress model which is formally comparable to a quadratic EVM. Since this model is a consequence of a differential second moment closure, no additional calibration of the coefficients is necessary. The purpose of the present paper is the assessment of these turbulence models with respect to model accuracy and robustness.

2. Mathematical model

The equations needed to describe steady, isothermal and incompressible turbulent flows using the Reynolds decomposition and subsequent averaging of flow quantities are the continuity and the Navier–Stokes equations, which read as follows in cartesian tensor notation.

$$\frac{\partial \bar{u}_i}{\partial x_i} = 0, \tag{1}$$

$$\frac{\partial \bar{u}_i}{\partial t} + \bar{u}_j \frac{\partial \bar{u}_i}{\partial x_j} = -\frac{1}{\rho}\frac{\partial \bar{p}}{\partial x_i} + \nu \frac{\partial^2 \bar{u}_i}{\partial x_j^2} - \frac{\partial \overline{u_i' u_j'}}{\partial x_j} + \bar{f}_i. \tag{2}$$

---

* Corresponding author. Tel.: +49-6151-16-6174; fax: +49-6151-16-4159.

E-mail address: haag@gfa.tu-darmstadt.de (O. Haag).

[1] Present address: AEA Technology GmbH, Staudenfeldweg 12, D-83624 Otterfing, Germany.

0142-727X/00/$ - see front matter
PII: S 0 1 4 2 - 7 2 7 X (0 0) 0 0 0 1 5 - 1

Turbulence models are necessary to determine the unknown Reynolds stress tensor $\overline{u_i'u_j'}$ appearing in the momentum equation (2). This can either be accomplished by deriving a transport equation for $\overline{u_i'u_j'}$ (and further modeling of the unknown terms there) or by developing a relationship between $\overline{u_i'u_j'}$ and known quantities of the mean flow. The first method leads to differential turbulence models (i.e., second moment closure models (SMC)) and will not be described in this context. The latter approach leads to algebraic turbulence models (i.e., EVMs) and will be discussed briefly in the next section.

3. Algebraic turbulence models

All algebraic turbulence models are based upon the assumption that the Reynolds stress tensor is only a function of the mean velocity gradient, one turbulent length scale and one turbulent time scale.

$$\overline{u_i'u_j'} = F\left[\frac{\partial \overline{u}_i}{\partial x_j}, l_t, t_t\right]. \tag{3}$$

The turbulent length and time scale are expressed in terms of the turbulent kinetic energy $k = (1/2)\overline{u_i'u_j'}$ and its dissipation rate ϵ. Eq. (3) can be non-dimensionalized using the Buckingham theorem (see Shih et al., 1995; Speziale, 1991). From this Shih et al. (1995) and Lumley (1978) developed a general constitutive relationship for the Reynolds stresses making use of the Cayley–Hamilton theorem. Eq. (4) shows this relation truncated at cubic order products terms of strain and vorticity tensors.

$$\begin{aligned}\overline{u_i'u_j'} &= \frac{2}{3}k\delta_{ij} - 2C_\mu \frac{k^2}{\epsilon}S_{ij} \\ &+ C_1\frac{k^3}{\epsilon^2}\left[S_{ik}S_{jk} - \frac{1}{3}S_{kl}S_{kl}\delta_{ij}\right] + C_2\frac{k^3}{\epsilon^2}\left[W_{ik}S_{jk} + W_{jk}S_{ik}\right] \\ &+ C_3\frac{k^3}{\epsilon^2}\left[W_{ik}W_{jk} - \frac{1}{3}W_{kl}W_{kl}\delta_{ij}\right] + C_4\frac{k^4}{\epsilon^3}\left[S_{ki}W_{lj} + S_{kj}W_{li}\right]S_{kl} \\ &+ C_5\frac{k^4}{\epsilon^3}\left[W_{il}W_{lm}S_{mj} + S_{il}W_{lm}W_{mj} - \frac{2}{3}S_{lm}W_{mn}W_{nl}\delta_{ij}\right] \\ &+ C_6\frac{k^4}{\epsilon^3}S_{ij}S_{kl}S_{kl} + C_7\frac{k^4}{\epsilon^3}S_{ij}W_{kl}W_{kl}.\end{aligned} \tag{4}$$

In Eq. (4) the mean velocity gradient is split into strain and absolute vorticity tensor (5), where Ω_k is the rotation rate of the coordinate system.

$$\begin{aligned}S_{ij} &= \frac{1}{2}\left[\frac{\partial \overline{u}_i}{\partial x_j} + \frac{\partial \overline{u}_j}{\partial x_i}\right] \quad \text{and} \\ W_{ij} &= \frac{1}{2}\left[\frac{\partial \overline{u}_i}{\partial x_j} - \frac{\partial \overline{u}_j}{\partial x_i}\right] - \epsilon_{ijk}\Omega_k.\end{aligned} \tag{5}$$

The coefficients C_i appearing in Eq. (4) are functions of the strain and vorticity tensor invariants. The various nonlinear EVMs can be characterized through the order of products of strain and vorticity tensor terms they incorporate in their stress strain relationship. They differ in the way the free coefficients of the constitutive relationship are calibrated. In the case of explicit algebraic turbulence models no additional calibration of the coefficients is necessary. Those turbulence models are derived from differential Reynolds stress models where the coefficients were modeled also.

Tables 1 and 2 are intended to give a short overview of how the different coefficients were modeled in the turbulence models considered here. From Table 1 one can see that most effort was spent for the calibration of the coefficient C_μ because through the linear term coefficient the ability of taking into account the extra rate of strain effects on turbulence is modeled.

The ability of the turbulence models to predict the effects of extra rates of strain like streamline curvature or Coriolis forces on turbulence can be analyzed in the case of a homogeneous turbulent shear flow with respect to a rotating frame according to Speziale (1989). In homogeneous shear flows the Reynolds stress anisotropy tensor $b_{ij} = \overline{u_i'u_j'}/2k - (1/3)\delta_{ij}$ and the dimensionless shear parameter Sk/ϵ achieve asymptotic equilibrium values for long dimensionless times ($t^* \to \infty$, $t^* = St$) that are almost independent of the initial conditions. The dimensionless shear parameter $(\epsilon/Sk)_\infty$ is through its dependence on the modeled shear component b_{12} a function of the non-dimensional rotation rate Ω/S in Eq. (6).

$$P_k = -2kb_{12}S \quad \text{and} \quad \frac{P_k}{\epsilon}\Big|_\infty = \frac{C_{\epsilon 2} - 1}{C_{\epsilon 1} - 1}. \tag{6}$$

The non-dimensional shear parameter $(\epsilon/Sk)_\infty$ is a characteristic parameter of turbulent kinetic energy budget (7):

$$\frac{k}{k_0} = \mathrm{e}^{\lambda t^*}, \quad \lambda = \frac{C_{\epsilon 2} - C_{\epsilon 1}}{C_{\epsilon 1} - 1}\left(\frac{\epsilon}{Sk}\right)_\infty. \tag{7}$$

If $(\epsilon/Sk)_\infty > 0$, then an exponential growth of the turbulent kinetic energy corresponding to an unstable flow is calculated ($C_{\epsilon 1} = 1.44$ and $C_{\epsilon 2} = 1.92$). Due to linear stability results from Speziale (1989) this exponential growth is only in the intermediate range $0.0 < \Omega/S < 0.5$ a stable solution. Outside this interval a decay of turbulent kinetic energy referring to a stabilizing Coriolis effects is observed. It is characterized by $(\epsilon/Sk)_\infty = 0$. This exchange of stabilities is illustrated in the bifurcation diagram in Fig. 1. Due to its material frame indifference the standard k–ϵ model does not account for any effect of Coriolis forces. For homogeneous turbulent flows the GS model represents exactly the underlying SMC calibrated for this flow (Gatski and Speziale, 1993). It predicts an unstable flow, corresponding to an increased turbulent momentum transfer in the interval $-0.07 < \Omega/S < 0.51$. Otherwise the flow is stable.

The altered turbulent momentum transfer predicted by the nonlinear SZL and CLS model is not limited to the rotation rate interval of the linear stability analysis. The SZL model predicts a higher dimensionless shear rate for $\Omega/S = 0$ than for $\Omega/S = 0.5$ according to the Richardson number similarity consideration of Speziale and MacGiolla Mhuiris (1989). A feature the CLS model does not obey. The CLS model can be improved by employing a modified absolute rotation rate tensor for the calibration of the linear term coefficient C_μ similar to those of the SZL or GS model.

4. Numerical method

The three-dimensional Reynolds averaged Navier–Stokes equations are discretized by an element based finite volume in a co-located variable arrangement. The coupled set of algebraic equations is solved by a coupled algebraic multigrid iterative solver (CFX-TfC) and the solution is accelerated by an algebraic multigrid. Details of the solution procedure can also be found in TASCflow theory documentation (1995) as both codes use the same computational approach. The major difference is that CFX-TfC works on unstructured grids also.

A proper linearization of the nonlinear stress representation is necessary as the momentum equations are strongly coupled through the nonlinear terms of the stress–strain relation. A purely lagged implementation alone and in combination with a relaxation of the higher order nonlinear terms (those terms multiplied with the coefficients C_1–C_7 in Eq. (4)) is highly

Table 1
The linear term coefficient[a]

	Model coefficient C_μ
k–ϵ	0.09
SZL	$\dfrac{1}{A_0 + A_s(k/\epsilon)\sqrt{S_2^2 + W_2^2}}$
CLS	$\dfrac{0.3}{1 + 0.35[\max(\tilde{S}_2, \tilde{W}_2)]^{1.5}}\left[1 - \exp\left(\dfrac{-0.36}{\exp\{-0.75\max(\tilde{S}_2, \tilde{W}_2)\}}\right)\right]$
GS	$0.233\dfrac{\left(\frac{4}{3} - C_2\right)1.5(1 + \eta^2)}{\left(3 + \eta^2 + 6\zeta^2\eta^2 + 6\zeta^2\right)}$

[a] Further definitions of parameters are left out for brevity.

Table 2
The higher-order term coefficients

	Model coefficients							
	C_μ	C_1	C_2	C_3	C_4	C_5	C_6	C_7
k–ϵ	(see Table 1)	–	–	–	–	–	–	–
SZL	(see Table 1)	–	$\dfrac{\sqrt{1 - 9C_\mu^2(k^2/\epsilon^2)S_2^2}}{1.0 + 6(k^2/\epsilon^2)S_2W_2}$	–	–	–	–	–
CLS	(see Table 1)	-0.1	0.10	0.26	$-10C_\mu^2$	–	$-5C_\mu^2$	$5C_\mu^2$
GS	(see Table 1)	6.8	0.36	1.25	0.4	–	–	–

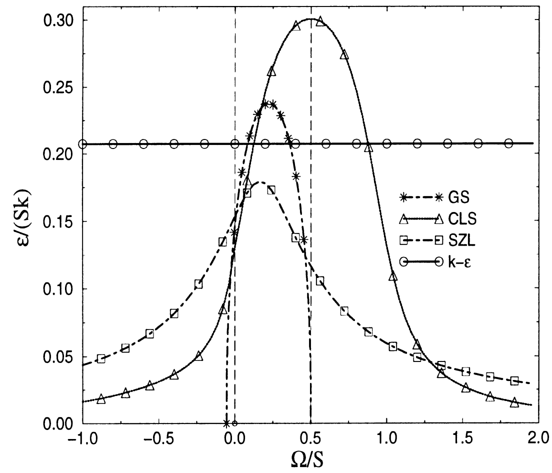

Fig. 1. Bifurcation diagram.

sensitive to the grid aspect ratio. These schemes converge for simple flows such as a plane boundary layer and plane turbulent channel flow but diverge for the calculation of more complex flows. The solvers' stability is not significantly increased once the inter equation coupling is implicitly accounted for by a Newton–Raphson linearization. A partly implicit scheme where the negative nonlinear parts are linearized and treated implicitly and treated explicitly as source terms otherwise does not improve situation much either. For the more complex test cases reported below, only a quasi-linear truncation of the nonlinear turbulence models yields grid independent converged solutions. The dependence of the coefficient C_μ on the mean strain and vorticity tensor invariants (see Table 1) was kept while all other coefficients (C_1–C_7) were neglected. This quasi-linear truncation turned out to be an efficient compromise between turbulence models ability of taking into account effects of extra rates of strain through a variable C_μ and necessary robustness of the solver. Problems with numerical stability in conjunction with the application of the GS model were also encountered by Abid et al. (1995) or Rahman et al. (1997) in their studies. Their approach was basically to modify the linear term coefficient instead.

The implemented turbulence models are verified by calculating a plane turbulent boundary layer and a plane turbulent channel flow. The model's capability to account for extra rate of strain effects is assessed by calculating three different test cases presented in the next section. In all test cases described, a converged solution was obtained if the sum of the maximum values for all residuals was below 10^{-4} for each transport equation. Grid independence studies ensured grid independent solutions in all cases. Starting from a coarse grid the number of elements in streamwise and wall normal direction was multiplied by the factors 2, 3 and 4 for finer grids. Grid independence was reached for indistinguishable solutions on different grid refinement levels. All solutions were obtained on block structured meshes with hexahedral elements. Boundary conditions for walls, inlets, outlets symmetry lines had to be specified. At walls the no-slip boundary condition was modeled with standard wall functions. At outflow symmetry boundaries zero gradient conditions for all variables were applied. At inlets profiles of measured flow variables were prescribed if available. Otherwise constant values for the flow properties had to be prescribed.

5. Results

Three situations are considered where streamline curvature has an influence on turbulent flow. A backward facing step flow investigated by Driver and Seegmiller (1985), a curved mixing layer from Castro and Bradshaw (1976) and the flow through a plane U-duct (Monson and Seegmiller, 1992). All flows are nominally two-dimensional. In all cases experimental data is available and is compared to the predictions of the different turbulence models.

5.1. Backward facing step

Driver and Seegmiller (1985) investigated the two-dimensional, steady, incompressible and turbulent flow at a backward facing step experimentally. The geometry is sketched in Fig. 2. The characteristic length of the geometry is the height of the step $H = 1.27$ cm. The characteristic velocity outside the boundary layer is $U_{\mathrm{ref}} = 44.2$ m/s resulting in a Reynolds number of $Re = 37\,423$.

The computational inlet is located $4H$ upstream of the step. To discretize the inlet region $(20 \times 40 \times 2)$ elements were used for the coarsest grid. The discretization of the downstream region consisted of $(50 \times 60 \times 2)$ elements on that level. Around the region of the measured reattachment point $(x/H = 6.26)$ the grid was refined. The computed reattachment length is an important parameter for the assessment of turbulence models in separated flows. Table 3 shows the comparison of computed and measured reattachment lengths for different turbulence models on the coarsest grid and the next grid refinement level. The CLS and the GS model compute the correct value for the reattachment length. The value for x/H is predicted too small by the standard k–ϵ and too large by the SZL model.

All turbulence models predict the main features (primary recirculation and corner vortex) of the flow. Fig. 3 shows the development of the pressure coefficient c_{p} along the lower wall in streamwise direction downstream of the step. The standard k–ϵ model predicts the rise of the pressure coefficient too early compared to experimental data. This is a consequence of the computed length of the recirculation zone being too small. All other models are in better agreement with experimental data because of their computed location of the reattachment point being in close agreement with experimental findings. Downstream of the reattachment point the overall pressure loss is computed correctly by the nonlinear EVMs but too small by the standard k–ϵ model. The general tendency of the nonlinear EVMs being in better agreement with experimental data for c_{p} calculations is confirmed by calculations of an adverse pressure gradient flow with recirculation bubble from Bauer et al. (1998) with the same models.

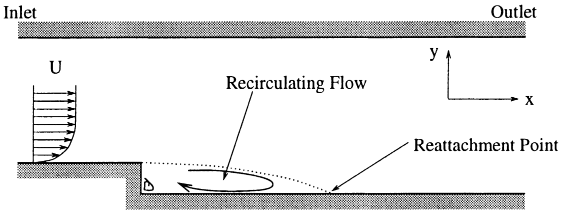

Fig. 2. Backward facing step flow.

The location of the reattachment point in Fig. 4 is characterized by $c_{\mathrm{f}} = 0$. Again the differences between linear and nonlinear EVMs can be observed in that region. But in contrast to the development of c_{p} the measured and computed development of c_{f} is not in good agreement for $x/H > 10$ and inside the recirculation zone. This is mainly a consequence of the standard wall functions used throughout the computations. Grotjans and Menter (1998) were able to compute the correct values for c_{f} using a standard k–ϵ model and a modified wall function approach. Other features of the flow like recirculation length or c_{p} distributions were not affected significantly with this approach.

A more detailed view of the turbulent flow field offer Figs. 5 and 6, where normalized mean velocity and turbulent kinetic energy are plotted at various locations x/H downstream the step. To achieve a compact graph the origin of every downstream profile was shifted 0.5 units along the abscissa with respect to its upstream profile. Profiles for turbulent kinetic energy in Fig. 6 were shifted 2.0 abscissa units. The velocity and turbulent kinetic energy distributions calculated with the nonlinear EVMs are remarkably indistinguishable from each other. Differences can only be seen compared to the k–ϵ model results in the recirculation region. Further downstream all models yield the same results.

The free shear layer thickness is underpredicted with the nonlinear EVMs compared to experimental data for the mean velocity distribution starting with position $x/H = 2$ downstream the step in Fig. 5. Results obtained with the linear model seem to be in slightly better agreement. This on the other hand leads to the above mentioned smaller value for the recirculation length. Downstream the recirculation zone none of the models is able to predict the flow acceleration near the bottom wall correctly.

Fig. 6 shows that all nonlinear EVMs predict very similar distributions of turbulent kinetic energy. Differences compared to the linear model are visible inside the recirculation zone. At $x/H = 4$ a maximum for k about $y/H = 0.5$ away from the bottom wall is measured which none of the models captures.

The nonlinear models overpredict the value of k at a bigger distance from the wall $(y/H = 0.7)$. The k–ϵ model calculates the maximum closer to the wall $(y/H = 0.6)$ with higher values for k compared to nonlinear model solutions. The differences are caused by differences in size and shape of the recirculation zone. Outside the recirculation zone $(x/h > 6.5)$ the decay of turbulence is only captured qualitatively since the level of turbulence predicted in the recirculation zone is too high for all models.

5.2. Curved mixing layer

Castro and Bradshaw (1976) investigated the influence of streamline curvature in a highly curved plain mixing layer experimentally. Fig. 7 shows a sketch of the experimental setup. Air is flowing through a nozzle with $D = 12.7$ cm towards a flat plate. The distance of nozzle exit and plate is $H = 44.7$ cm. After the nozzle exit a plain, free mixing layer develops. The presence of the plate causes the oncoming mixing layer to bend away before impinging onto the plate

Table 3
Comparison of reattachment lengths

	x/H				
	Data	k–ϵ	SZL	CLS	GS
$(20 \times 40 + 50 \times 60) \times 2$	6.3	5.9	7.1	6.8	6.5
$(40 \times 80 + 100 \times 120) \times 2$	6.3	5.8	6.8	6.4	6.3

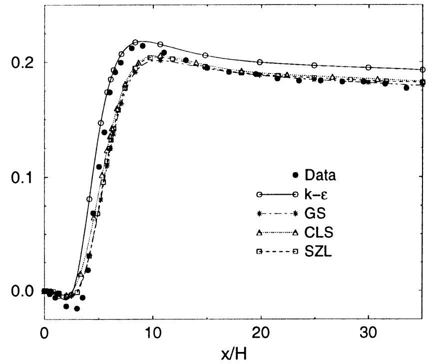

Fig. 3. Pressure coefficient c_p.

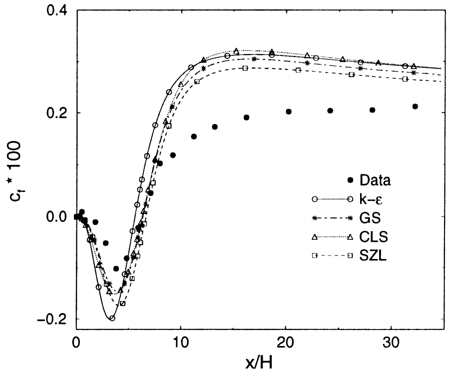

Fig. 4. Skin friction coefficient c_f.

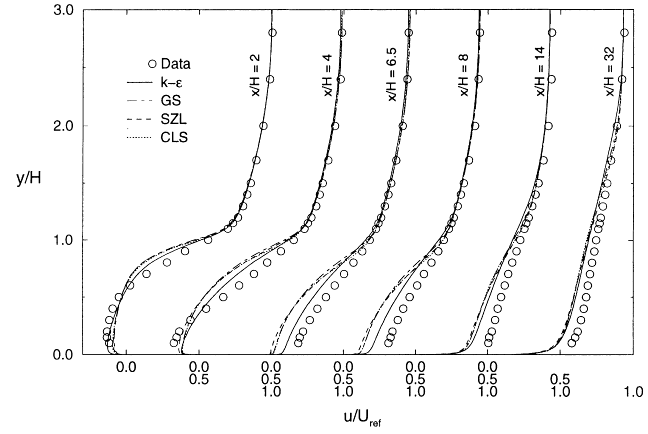

Fig. 5. Mean velocity distributions.

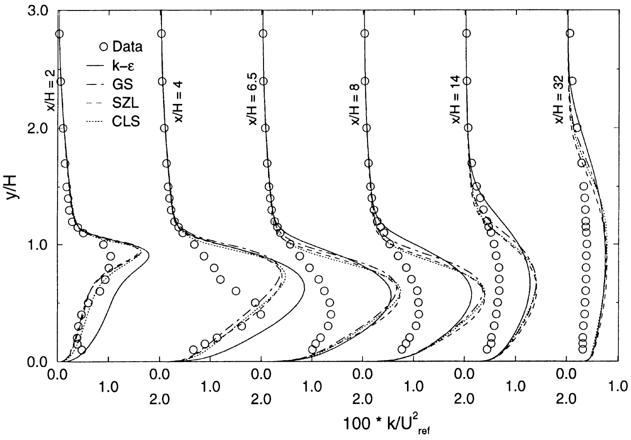

Fig. 6. Turbulent kinetic energy distributions.

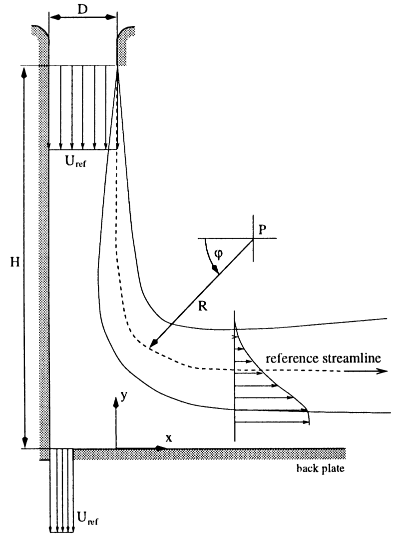

Fig. 7. Curved mixing layer flow.

resulting in a curved mixing layer. A boundary layer separation along the inner wall close to the stagnation point region is avoided through the presence of an outflow of width $W = 4$ cm in the back plate.

In this case no profiles for mean and turbulence properties at the inlet are available. Therefore constant values for velocity $U_{\text{ref}} = 33$ m/s, turbulent intensity $I = 0.001$ and a typical lengthscale for the energy containing eddies $l_t = 1$ cm were prescribed. The first calculations showed however, that these assumptions were not sufficient to approximate the situation at the nozzle inlet properly. Following the approach of Gibson and Rodi (1981) and Rodi and Scheuerer (1983) the computed distributions of velocity and turbulent kinetic energy of a free mixing layer with a mixing layer thickness $\delta = 3$ mm were prescribed at nozzle inlet instead of constant values.

Fig. 8 shows the development of mixing layer thickness δ along the length of a reference streamline. For angles $\varphi > 40°$ a decreased spreading rate of δ compared to spreading rates of free mixing layers is observed. This is a consequence of the stabilizing effects of convex streamline curvature on turbulence. Downstream the curved section the spreading rate increases again and reaches values that are slightly higher compared to values for free mixing layers. Results obtained with the standard k–ϵ model show a slight reduction of spreading rate in the curved section. The nonlinear EVMs are generally more sensitive towards curvature effects. The reduction in spreading rate is predicted higher than with the standard k–ϵ model. None of the turbulence models predicts the correct values for the spreading rates downstream the curved section. This is consistent with calculations of free mixing layers where also all models predict too small values for the spreading rate as well. In fact the standard k–ϵ model is closer to experimental data than the nonlinear EVMs in that region. In Fig. 9 the maximum values of radial distributions of normalized turbulent kinetic energy along the reference streamline can be seen. All models show the stabilizing effect of streamline curvature qualitatively correct. Again the nonlinear

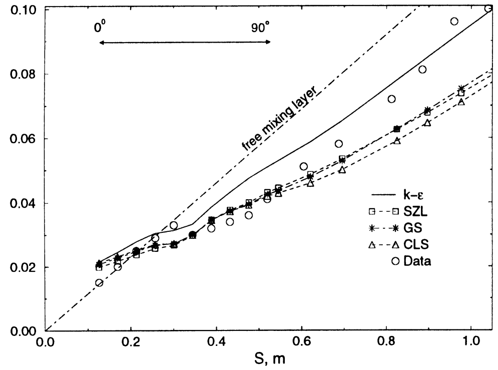

Fig. 8. Mixing layer thickness δ vs. length of reference streamline S.

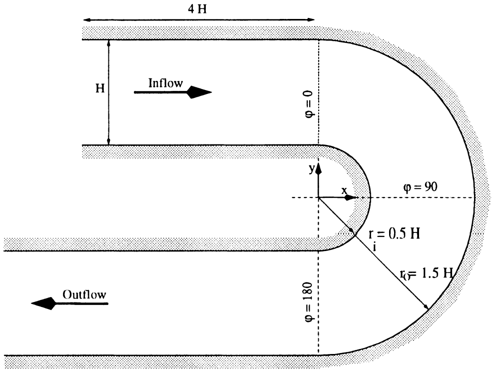

Fig. 10. Plane U-duct flow.

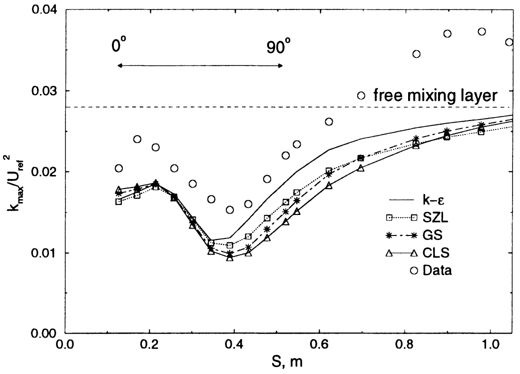

Fig. 9. Maximum k vs. length of reference streamline S.

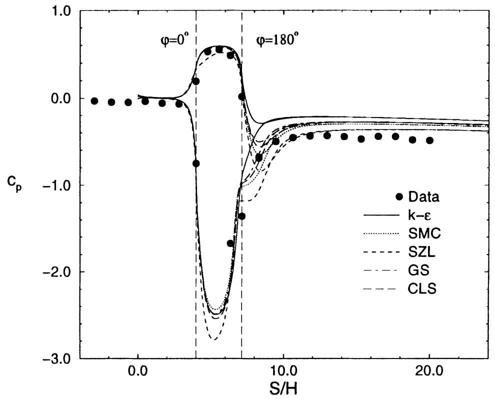

Fig. 11. Streamwise development of pressure coefficient c_p.

EVMs are more sensitive towards effects of streamline curvature than the linear EVM. The location of maximum damping of turbulent kinetic energy occurs at $\varphi \approx 60^\circ$ which is in good agreement with the predictions of the nonlinear EVMs. The standard k–ϵ model predicts the location of maximum damping too early and not as pronounced as the other models. The generally higher values for k predicted with the standard k–ϵ model are the reason for the higher values of spreading rate observed in Fig. 8. None of the models predicts the measured "overshooting" of turbulent kinetic energy downstream the curved section, but the asymptotic behavior of k far downstream the curved section towards the value of the free mixing layer ($k_{\max}/U_{\text{ref}}^2 = 0.028$) is both seen experimentally as well as computationally with all turbulence models.

5.3. Plane U-duct

Monson and Seegmiller (1992) investigated a low speed internal flow in a strongly curved U-duct. Fig. 10 shows a sketch of the experimental setup.

The Reynolds number based on the channel height $H = 3.81$ cm is $Re = 1 \times 10^6$. The basic grid is $(100 \times 10 \times 2)$ hexahedral element grid. Results presented below were obtained on a $(400 \times 80 \times 2)$ hexahedral element grid.

Fig. 11 shows the pressure distribution at the inner and outer wall in streamwise direction S normalized with channel height H. The value of $S/H = 0$ corresponds to the computational inlet which is located 4 duct heights upstream the bend. Outlet boundary conditions were specified 37 duct heights downstream the bend $S/H = 44$. In the first half of the curved section the mean flow is accelerated along the inner wall and decelerated along the outer wall. In the second half the situation is reversed. The flow accelerates along the outer wall and decelerates along the inner wall until finally the flow separates from the inner wall and a recirculation zone forms downstream the curved section. Results obtained with the CLS and the GS model are very similar to those of the SMC. The SZL model is highly sensitive to adverse pressure gradient conditions. It predicts the highest pressure loss of all models employed as it over-predicts the length of the separation zone. Conversely the predict overall pressure loss is lowest with the k–ϵ model. This is due to the fact that the k–ϵ model does not predict the separation bubble at the end of the bend.

This can be seen more clearly in Fig. 12. It shows the spanwise distribution of the mean streamwise velocity $\bar{u}$ from the inner ($y/H = 0$) to the outer ($y/H = 1$) duct wall at different axial locations. Since the mean velocity field in the bend is dictated by strong pressure gradients (see Fig. 11) results obtained with the different turbulence models are almost indistinguishable from each other and generally in good agreement with measured data. Only close to the concave duct wall discrepancies between measurements and calculations are present. This might be attributed to the fact that the models generally fail to predict the high degree of turbulent mixing bringing high momentum fluid from the core flow close to the outer wall.

Negative values for $\bar{u}$ at $\varphi = 180^\circ$ indicate the separation zone which, as mentioned before, is captured by all nonlinear type models. Only the k–ϵ model does not predict a separation bubble. Further downstream the maximum of the mean streamwise velocity has shifted from the inner towards the outer duct wall because the separation bubble reduces the effective through flow area and leads to to flow acceleration there. Contrary to all other models considered the k–ϵ model predicts a qualitatively wrong velocity distribution. This is a direct result of its inability to predict the separation zone. The main reason for the different predictive quality of the turbulence models is their ability to take into account curvature effects on turbulence which will now be discussed in more detail. But another reason worth being mentioned is the modeling of the near wall turbulence. Luo and Lakshminarayana (1995) for instance were able to calculate a (although very small) recirculation zone even with the k–ϵ model in their very detailed study of this flow because they used a one-equation model to model near wall turbulence. Grotjans et al. (1999) also successfully computed a recirculation zone with the k–ϵ model. They used their previously mentioned modified wall function approach.

Fig. 13 respectively shows the distributions of the turbulent kinetic energy k at the same axial positions. Streamline curvature causes a damping of turbulence at the convex, inner duct wall and augmentation at the concave, outer wall. This can be seen for instance at position $\varphi = 90°$ in Fig. 13. All models except the linear one predict this behavior at least qualitatively correct. The damping of turbulence is captured quite satisfactory while the augmentation is under-predicted compared to experimental values. This might be the reason for the previously mentioned discrepancies in measured and calculated mean velocity distributions near the concave wall at $\varphi = 90°$ in Fig. 12.

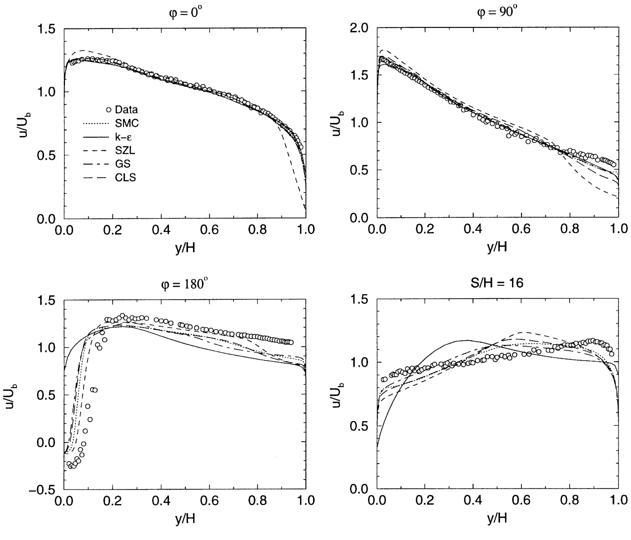

Fig. 12. Spanwise mean velocity distributions at different axial locations.

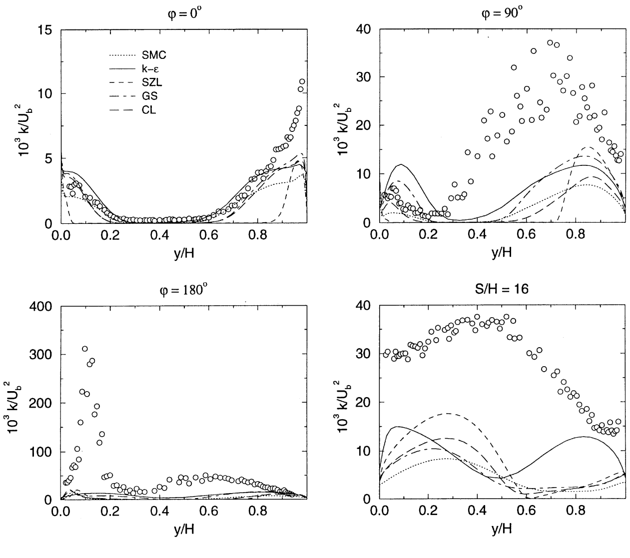

Fig. 13. Spanwise kinetic energy distributions at different axial locations.

With the k–ϵ model the maximum values for k are equally high both near the convex and the concave duct wall. This is due to its constant linear term coefficient C_μ (see Table 1). Consequently no separation is predicted downstream the bend because the damping of turbulence together with flow deceleration in the second half of the bend lead to flow separation. Because of the transient conditions of the separation bubble the measured values for k are extremely high and are not captured by any of the models. The nonlinear EVMs predict an altered turbulent transport through their variable linear term coefficients and therefore a separation zone is calculated similar to that calculated by the SMC. Further downstream the situation does not improve.

The nonlinear models (and the SMC) predict a qualitatively correct distribution for k with much lower values for k compared to experimental data while the linear model predicts it even qualitatively incorrect.

The CPU time of the turbulent U-duct flow calculations is for nonlinear EVMs in the range of 0.9–1.4 times that necessary for standard $k - \epsilon$ calculations in all grid resolutions considered. For SMC calculations a factor 2.1–4.6 is observed.

6. Conclusions

Three nonlinear EVMs have been assessed with respect to accuracy of flow predictions and computational robustness in flows where curvature alters turbulent momentum transport. Due to curvature secondary strain components become more important resulting in high cross-velocity coupling of the momentum equations which finally leads to solver divergence. Under-relaxation of the nonlinear terms and different linearization schemes cannot cure the problem. Truncation of the nonlinear EVM at first order leaves the quasi-linear models capable in accounting for the altered turbulent momentum transport through the dependence of the linear model term coefficient C_μ on the strain and vorticity tensor invariants. As these truncated EVMs are of tensorially linear order they cannot predict different magnitudes of normal Reynolds stress components, but extra rates of strain effects on the shear components are modeled in a manner similar to cubic nonlinear EVMs. Results show that for more complex flows with separation the presence of recirculation zones is highly influential for the entire turbulent flow field and that the nonlinear EVMs are able to predict such major flow features more precisely than the k–ϵ model, which in the case of the U-duct flow cannot predict a recirculation zone at all. Therefore the quasi-linear EVMs offer an improvement in accuracy of flow predictions compared to standard k–ϵ calculations with a moderate increase in CPU-time. Computational robustness is only slightly decreased compared to standard k–ϵ calculations. The combination of accuracy and robustness makes the nonlinear EVMs a promising candidate especially for industrial flow applications. Results also indicate that care has to be taken when specifying inflow boundary conditions as well as wall boundary conditions because their influence can exceed the influence of turbulence modeling on accuracy of flow calculations.

Acknowledgements

The authors wish to acknowledge the support by AEA Technology GmbH and the Deutsche Forschungsgemeinschaft (DFG) through their sponsorship of *Graduiertenkolleg Modellierung und numerische Beschreibung technischer Strömungen*.

References

Abid, R., Rumsey, C., Gatski, T., 1995. Prediction of nonequilibrium turbulent flows with explicit algebraic stress models. AIAA J. 33 (11), 2026–2031.

Advanced Scientific Computing Ltd., 1995. TASCflow theory documentation, 2.4 edition. ASC, Waterloo, Canada.

Bauer, W., Haag, O., Hennecke, D., 1998. Comparison of different nonlinear eddy viscosity models for engineering applications. In: Papailou, K., Tsahalis, D., Periaux, J., Hirsch, C., Pandolfi, M. (Eds.), Computational Fluid Dynamics '98, vol. 1. Wiley, New York, pp. 1099–1104.

Castro, I.P., Bradshaw, P., 1976. The turbulent structure of a highly curved mixing layer. J. Fluid Mech. 73, 265–304.

Craft, T.J., Launder, B.E., Suga, K., 1996. Development and application of a cubic eddy-viscosity model of turbulence. Int J. Heat Fluid Flow 17, 108–115.

Driver, D.M., Seegmiller, H.L., 1985. Features of a reattaching turbulent shear layer in divergent channel flow. AIAA J. 23, 163–171.

Gatski, T.B., Speziale, C.G., 1993. On explicit algebraic stress models for complex turbulent flows. J. Fluid Mech. 254, 59–78.

Gibson, M.M., Rodi, W., 1981. A Reynolds-stress closure model of turbulence applied to the calculation of a highly curved mixing layer. J. Fluid Mech. 103, 161–182.

Grotjans, H., Menter, F., Burr, R., Glück, M., 1999. Higher order turbulence modelling for industrial applications. In: Rodi, W., Laurence, D. (Eds.), Engineering Turbulence Modelling and Experiments 4. Elsevier, Amsterdam, pp. 269–278.

Grotjans, H., Menter, F.R., 1998. Wall functions for general application CFD codes. In: Papailou, K., Tsahalis, D., Periaux, J., Hirsch, C., Pandolfi, M. (Eds.), Computational Fluid Dynamics '98, vol. 1. Wiley, New York, pp. 1112–1117.

Lumley, J.L., 1978. Computational modeling of turbulent flows. Adv. Appl. Mech. 18, 123–176.

Luo, J., Lakshminarayana, B., 1995. Prediction of strongly curved turbulent duct flows with Reynolds stress model. In: 26th AIAA Fluid Dynamic Conference, San Diego, CA. Technical Report, AIAA-95-23241, June.

Monson, D.J., Seegmiller, H.L., 1992. An experimental investigation of subsonic flow in a two-dimensional u-duct. NASA Technical Memorandum, 103931.

Rahman, M., Rautaheimo, P., Siikonen, T., 1997. Numerical study of turbulent heat transfer from a confined impinging jet using a pseudo-compressibility method. In: Hanjalić, K., Peeters, T. (Eds.), Turbulence, Heat and Mass Transfer 2. Delft University Press, Delft, pp. 511–520.

Rodi, W., Scheuerer, G., 1983. Calculation of curved shear layers with two equation turbulence models. Phys. Fluids 26, 1422–1436.

Shih, T.H., Zhu, J., Lumley, J.L., 1995. A new Reynolds stress algebraic equation model. Comput. Methods. Appl. Mech. Engrg. 125, 287–302.

Speziale, C.G., 1989. On the prediction of equilibrium states in homogeneous turbulence. J. Fluid Mech. 209, 591–615.

Speziale, C.G., 1991. Analytical methods for the development of Reynolds-stress closures in turbulence. Annu. Rev. Fluid Mech. 23, 107–157.

Speziale, C.G., MacGiolla Mhuiris, N., 1989. Scaling laws for homogeneous turbulent shear flows in a rotating frame. Phys. Fluids A 1, 294–301.